Computers and Fluids 120 (2015) 37–45

Contents lists available at ScienceDirect

Computers and Fluids

journal homepage: www.elsevier.com/locate/compfluid

Lattice-Boltzmann modeling of unstable flows amid arrays of wires

G. Boroni [a], N. Silin [b], D. Dalponte [a], J. Dottori [a], A. Clausse [a,*]

[a] CONICET-CICPBA-CNEA and National University of Central Buenos Aires, 7000 Tandil, Argentina
[b] CONICET and Instituto Balseiro, 8400 Bariloche, Argentina

ARTICLE INFO

Article history:
Received 19 September 2014
Revised 13 July 2015
Accepted 21 July 2015
Available online 3 August 2015

Keywords:
Lattice Boltzmann method
Permeable media
Flow instability
Flow correlation
Coherent structures
Wires

ABSTRACT

A lattice-Boltzmann model (LBM) of unstable flows amid easily permeable obstructions consisting of regular arrays of wires is presented. The obstacles are modeled by forces incorporated as source terms in the LBM equation, following the same procedure as the immersed boundary method. Yet the present method differs from the latter in that the structure is represented by a volumetric array of fixed points. Also each structural point exerts reactive forces governed by the Darcy law, rather than by elastic kinematics. The model is validated against two experiments consisting of air flowing in a channel partially obstructed by arrays of wires, finding excellent agreement. The simulations reveal the formation of complex vortical structures amid the wired region, which can be of interest in understanding natural phenomena or practical applications.

© 2015 Elsevier Ltd. All rights reserved.

1. Introduction

The numerical modeling of flows in easily permeable media, like the flow amid complex arrays of small obstacles, is a challenging task. This kind of flows occurs in a number of interesting cases, like fluid currents around crops or aquatic plants [6,13,21]. In technological applications they are encountered for example in the cooling of electronic components. A comprehensive review on compound channels and flows parallel to rod bundles can be found in Meyer [15].

An interesting feature of these flows is that they easily become unstable in the boundaries between the permeable regions and the free flow [28]. This instability is associated to inflexion points of the velocity profile, and manifests as coherent wavy and vortical structures that amplify the momentum and scalar transversal diffusion [3,18]. These structures are useful for they modify the transport of scalars not only at the interface where structures are generated, but also inside and outside the obstruction, favoring processes such as pollination, nutrient transport, and heat and mass transfer [5,23]. A number of recent analytical studies have been aimed to characterize the stability of partially permeable channels [14,24,25,28].

From the point of view of modeling, finding adequate representations of the arrays of obstacles, that capture the characteristics of the mentioned instabilities while keeping reasonable computational costs, is not a trivial task. The lattice Boltzmann method (LBM) has shown an impressive versatility to model porous media and flows through regions partially blocked by obstacles ([19,7,10,27]). For a good review of applications of LBM to porous media (see Sukop and Thorne [26]). Moreover, recently it has been shown that flow instabilities in cavities can be simulated using LBM [2,8].

The present article reports the modeling of the sustained oscillatory flow in a channel with low Reynolds number partially obstructed by an array of wires. The wired region is modeled by Darcy-like forces imposed around the location of each wire. This is a major difference from a previous approach based on local bounce-back corrections, which produced less accurate results and introduced spurious mass sources [4]. The model is validated against two experiments consisting of air flowing in a channel partially obstructed by arrays of wires in different configurations.

2. Modeling

From the numerical point of view, LBM can be seen as an explicit method to solve transport equations using more variables than the strictly necessary to characterize the macroscopic flow. It is based on the movement and collision of pseudo-particles described by the lattice–Boltzmann equation:

$$f_i(\vec{x}+\vec{e}_i\Delta x, t+\Delta t) = f_i(\vec{x},t) - \frac{1}{\tau}\left[f_i(\vec{x},t) - f_i^e(\vec{x},t)\right] + S_i(\vec{x},t), \text{ for } i = 0,\ldots,\ell-1 \quad (1)$$

where $f_i(\vec{x},t)$ and $S_i(\vec{x},t)$ represent the particles distribution density and source at position $\vec{x}$ and time t, undergoing a displacement $\vec{e}_i\Delta x$ in a time step Δt. The vectors $\vec{e}_i$ form a finite set of ℓ lattice directions

* Corresponding author. Tel.: +54 249 4425817/4385690; fax: +54 249 4385690.
E-mail address: clausse@exa.unicen.edu.ar (A. Clausse).

http://dx.doi.org/10.1016/j.compfluid.2015.07.026
0045-7930/© 2015 Elsevier Ltd. All rights reserved.

that restrict the movement of the particles. In what follows the so called D2Q9 model will be used, which approach to second order the two-dimensional Navier–Stokes equations and is given by the set:

$$\vec{e}_0 = (0,0);\ \vec{e}_1 = (1,0);\ \vec{e}_2 = (0,1);\ \vec{e}_3 = (-1,0);\ \vec{e}_4 = (0,-1);$$
$$\vec{e}_5 = (1,1);\ \vec{e}_6 = (-1,1);\ \vec{e}_7 = (-1,-1);\ \vec{e}_8 = (1,-1). \quad (2)$$

Using an asymptotic expansion, it has been demonstrated that the LBE approximates the Navier–Stokes equations, provided that the so called equilibrium function $f_i^e(\vec{x},t)$ satisfies a set of constitutive conditions related to the moments of $f_i(\vec{x},t)$ respect to $\vec{e}_i$. Comprehensive reviews of this procedure can be found elsewhere [9,22,29]. A popular scheme complying with these conditions is the classical BGK, which for D2Q9 is given by:

$$f_i^e(\vec{x},t) = w_i\rho\left[1 + 3\frac{(v\vec{e}_i\cdot\vec{u})}{v^2} - \frac{3}{2}\frac{u^2}{v^2} + \frac{9}{2}\frac{(v\vec{e}_i\cdot\vec{u})^2}{v^4}\right], \quad (3)$$

where $v = \Delta x/\Delta t$ is the particle speed and:

$$\rho = \sum_i f_i(\vec{x},t) \text{ and } \vec{u} = \frac{1}{\rho}\sum_i v\vec{e}_i f_i(\vec{x},t) \quad (4)$$

are the particle-number density and average velocity. The coefficients w_i are 4/9 for the resting particles, 1/9 for the Cartesian directions and 1/36 for the diagonal directions. In such case, the relaxation parameter τ is related to the kinematic viscosity of the fluid by:

$$\upsilon = (2\tau - 1)\ \Delta x^2/(6\Delta t) \quad (5)$$

and the pressure is calculated using the isothermal pseudo equation of state:

$$p = \frac{1}{3}\rho v^2. \quad (6)$$

The term$S_i(\vec{x},t)$ is generally used to account for external forces. There is certain flexibility to manage this term. In the present work, it is assumed that a volumetric force $\vec{F}(\vec{x},t)$ can be applied in each cell, and the following expression recommended by Mohamad & Kuzmin [16] will be used:

$$S_i(\vec{x},t) = 3\frac{\Delta t}{v}w_i\vec{e}_i\cdot\vec{F}(\vec{x},t). \quad (7)$$

In effect, contracting the velocity index of S_i and $\vec{e}_i S_i$ yields:

$$\sum_i S_i = 3\frac{\Delta t}{v}\sum_i w_i\vec{e}_i\cdot\vec{F} = 0 \quad (8)$$

which ensures mass conservation, and

$$\sum_i v\vec{e}_i S_i = 3\ \Delta t\ \sum_i w_i\ \vec{e}_i\otimes\vec{e}_i\cdot\vec{F} = 3\Delta t\begin{pmatrix}1/3 & 0\\ 0 & 1/3\end{pmatrix}\cdot\vec{F} = \Delta t\vec{F} \quad (9)$$

provides the momentum bit to the cell driven by the volumetric force.

2.1. Model of the permeable media with LMB

The permeable media was simulated by means of source terms accounting for the drag forces imposed by the array of obstacles in the channel. The rationale behind this method is to simulate the Darcy's law, which states that the volumetric drag force $\vec{F}_D$ of permeable media is given by:

$$\vec{F}_D = -\frac{\rho\upsilon}{\kappa}\vec{u} \quad (10)$$

where κ is the permeability of the media.

The direct way to incorporate Darcy's law in LBM is to distribute the force uniformly in each cell of the permeable region, by introducing Eq. 10 in the source term. Although this is attractive for its simplicity, the numerical tests showed significant differences with the experimental data, particularly in transient and unstable conditions. In the present case, the main reason of the poor performance of a homogeneous model of forces is that the actual permeable media where the experiments were carried out is not homogeneous but it is composed by discrete thin wires that oppose to the flow locally. In order to simulate more closely the wire array while maintaining the simplicity of Darcy's law, another model is proposed in which the force term is applied in the neighborhood of each wire location. This is implemented following the same procedure as in the immersed-boundary method (IBM) used in fluid-structure interaction schemes [20,1].

In IBM the fluid is represented on an Eulerian coordinate whereas structures are represented by collections of parametric curves or surfaces on a Lagrangian coordinate. The forces exerted by the immersed boundary on the fluid are incorporated as source terms in the fluid equation via smooth approximations of the Dirac δ distribution. The immersed boundary is considered as a massless elastic fiber or membrane that moves with the local fluid velocity interpolated with the same δ distribution approximation.

In the present approach permeable structures are coupled with the fluid through smooth approximations of the δ distribution as in IBM. However, the present method differs from IBM in that the structure is represented by volumetric arrays of fixed points on the same Eulerian coordinate grid as the fluid, over which each structural point exerts reactive forces governed by the Darcy law rather than by elastic kinematics. The permeable region is accordingly defined by a set of reference points x_k, each of which introduces a source term $S_{ki}(\vec{x},t)$to the cells located in its neighborhood, given by:

$$S_{ki}(\vec{x},t) = -3\frac{\Delta t}{v}\ \frac{\rho\upsilon}{\kappa}\ N_k\delta(\vec{x}_k,\vec{x})\ w_i\ \vec{e}_i\cdot\overrightarrow{u}_k \quad (11)$$

where N_k is the number of LB cells that constitute a unit cell of the permeable media and

$$\delta(\vec{x}_k,\vec{x}) = \begin{cases} C(r)\left[1+\cos\dfrac{\pi(x-x_k)}{r\,\Delta x}\right]\left[1+\cos\dfrac{\pi(y-y_k)}{r\,\Delta x}\right] \\ \qquad if\ \left|\dfrac{(x-x_k)}{r\,\Delta x}\right| and \left|\dfrac{(y-x_k)}{r\,\Delta x}\right| < 1 \\ 0 \quad \text{otherwise} \end{cases}. \quad (12)$$

In other words, the force is distributed among the cells located at a distance $r\Delta x$ in each direction from the reference point. The radius of influence r is used for calibration purposes and it is expected to depend on the obstacle specifics (shape, size, roughness, etc.). $C(r)$ is a normalization factor given by:

$$C(r) = \left[\sum_{n=-r}^{r}\left(1+\cos\frac{\pi n}{2r}\right)\right]^{-2}. \quad (13)$$

The characteristic velocity of the neighborhood $\vec{u}_k$ is defined as:

$$\vec{u}_k = \sum_{\vec{x}}\delta(\vec{x}_k,\vec{x})\ \vec{u}(\vec{x}). \quad (14)$$

In Eq. (14) the summation is performed over all the cells of the grid, although the factor $\delta(\vec{x}_k,\vec{x})$ restricts the effect only to the cells within the zone of influence of the reference point $\vec{x}_k$.

3. Experiment

An experimental setup was constructed in order to provide a reference case and reliable measurements to compare with the numerical model. The test section, shown in Fig. 1, is a rectangular channel with transparent acrylic walls. The working fluid is ambient air that enters the channel from one end and is forced out by a fan located on the other end. The obstructed region consists of a regular array of copper wires lined horizontally across the test section, occupying

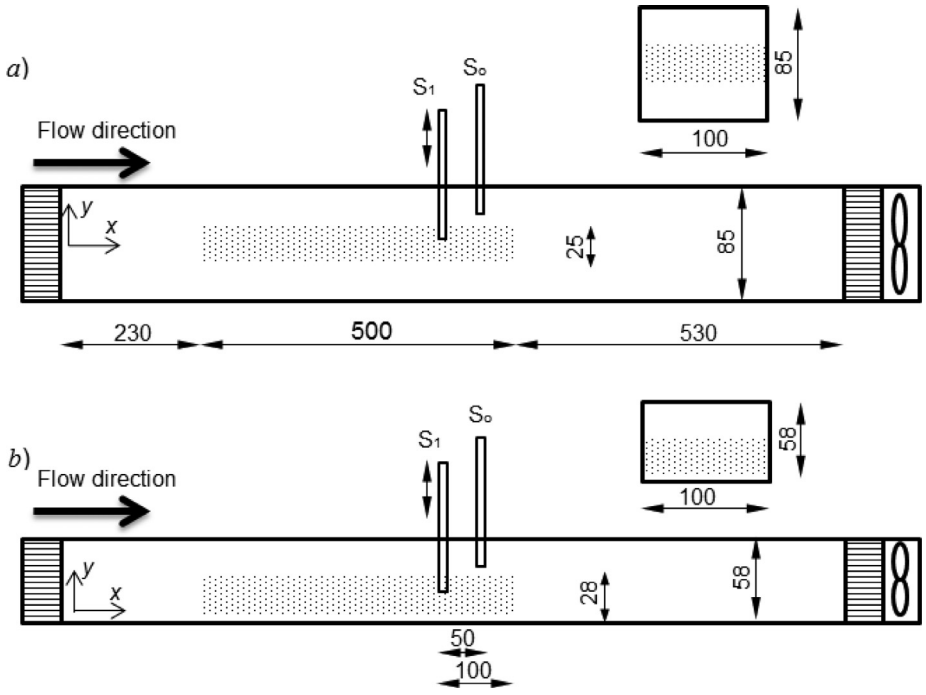

Fig. 1. Experimental Setup, (*a*) central obstruction, (*b*) lateral obstruction.

only a part of the channel cross section (Fig. 1). The diameter of the wires is 0.25 mm and the spacing between wires is 5 mm measured between centers in the flow direction and 2.5 mm in the transversal direction. The dimensions and separation between the wires permit the insertion of a probe in between, but it is sufficiently small as to avoid vortex shedding from the wires or flow channeling. A detailed description of the dimensioning criteria can be found in Silin et al. [24].

A honeycomb and a fine metallic mesh are used at the inlet to obtain a uniform entrance velocity field. Another honeycomb is placed 2 cm before the outlet fan to avoid upstream back swirls. One of the walls was placed in two different positions (Fig. 1), either adjacent to the wired obstruction on one side leaving a free flow passage on the other side (lateral configuration), or leaving two symmetric free flow passages on both sides of the wired region (central configuration).

Velocity measurements were obtained by means of constant-temperature hot-wire anemometers (CTA) placed in strategic positions along the channel at the symmetry plane, i.e., at the center of the span wise direction. The wires of the anemometers were oriented perpendicular to the main flow direction to achieve high sensibility for the axial velocity component but low sensibility for the transversal velocity component. The CTA was operated with a 0.5 overheat ratio and all measurements were done at ambient temperatures between 21 and 22 °C. Details of the CTA electronics can be found in Osorio et al. [17]. The Reynolds numbers were kept much lower than the critical value for rectangular channels [11]. The data were acquired by means of a 12 bit analog/digital converter board connected to a personal computer. Each measurement realization recorded 20,000 samples (20 s, 1 kHz) for velocity profiles and 60,000 (60 s, 1 kHz) for correlations between probes.

4. Results

The LBM model of permeable media was applied to simulate the gas flow in the rectangular channel blocked by a wired obstruction placed in the lateral and central configurations, as described in the previous section. No-slip boundary conditions were imposed at the walls, and uniform velocity and density were imposed at the inlet and exit respectively, following the scheme proposed by Zou and He [30]. Table 1 lists the parameter values used in the calculations. The Reynolds number is defined as:

Table 1
Lattice Boltzmann parameters used in the numerical simulations.

Obstruction	Lateral	Central
Grid size	2440 × 116	2440 × 170
N_k	50	50
τ	0.56	0.56
Inlet velocity (cm/s)	12.1	16.5

$$\mathrm{Re} = \frac{u_i h}{\upsilon}, \tag{15}$$

where u_i is the inlet velocity, h is the channel width and υ is the kinematic viscosity. After a sensibility analysis the grid resolution was chosen such that doubling the number of cells results in a maximum variation of the l^2 norm of the velocity at any cell within 1%.

The first task was to determine the numerical parameters representing the permeable region. This was done by adjusting the values of r and κ in order to reproduce the profiles of the average axial velocity measured in steady state. Since the flow at the working Reynolds numbers is unstable, the steady state corresponds to a sustained oscillation of the velocity. Consequently, the average velocity and the standard deviation of the fluctuations were used as reference for the calibration. Figs. 2 and 3 show the comparison of the numerical axial velocity profile in permanent flow regime with the corresponding measurement at the reference probe location x_o, for the lateral and central configuration respectively. It can be seen that the experimental profiles of velocity and the velocity fluctuations in both cases could be reproduced successfully in the numerical simulation. The differences in some regions can be traced both to imperfections in the experimental device, as well as microscopic effects that arise in cylinder arrays, which make the homogeneous assumption not perfectly valid [12]. The dashed curves correspond to the numerical results obtained by imposing a 0.1% perturbation on the inlet velocity to check

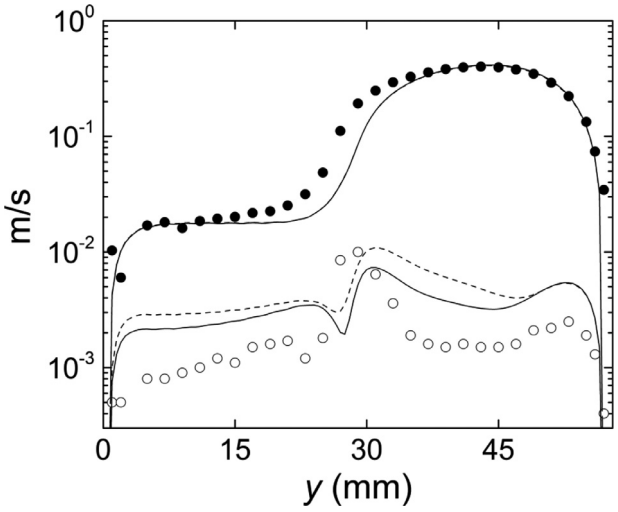

Fig. 2. Transversal profile of the mean velocity (•) and the standard deviation of the velocity fluctuations (o) for the lateral configuration. The profile was taken at a position x_o 50 mm downstream the end of the permeable region. The curves correspond to the numerical calculation with constant inlet velocity (solid) and a perturbation of 0.1% at the inlet (dashed).

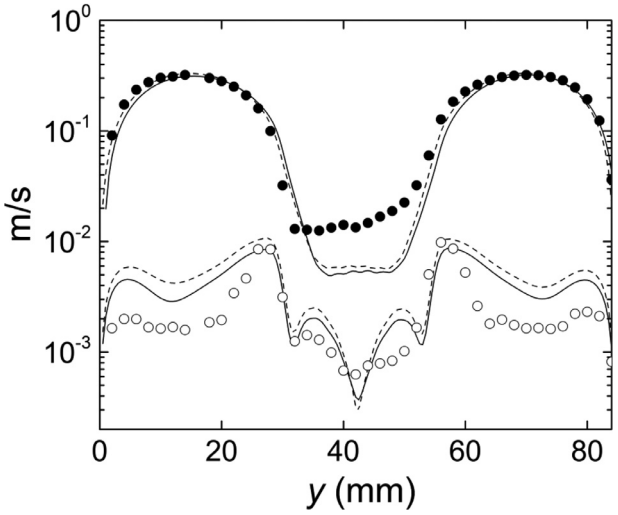

Fig. 3. Transversal profile of the mean velocity (•) and the standard deviation of the velocity fluctuations (o) for the central configuration. The profile was taken at a position x_o 50 mm downstream the end of the permeable region. The curves correspond to the numerical calculation with constant inlet velocity (solid) and a perturbation of 0.1% at the inlet (dashed).

the sensitivity of the results. It can be observed that the amplification factor is large for the standard deviation, which reinforce the importance of the design of the inlet section of this type of flows. The best fit was obtained for $r = 2$ and $\kappa = 1.45\ 10^{-4}\ m^2$. It should be stressed that the same values of r and κ were used for both arrangements of wires, which indicates that the parameters are determined mainly by the characteristics of the penetrable media, given in present case by the diameter of the wires and their spacing.

Figs. 4 and 5 show the contour maps of the average stream-wise and transversal velocity, and the corresponding standard deviations,

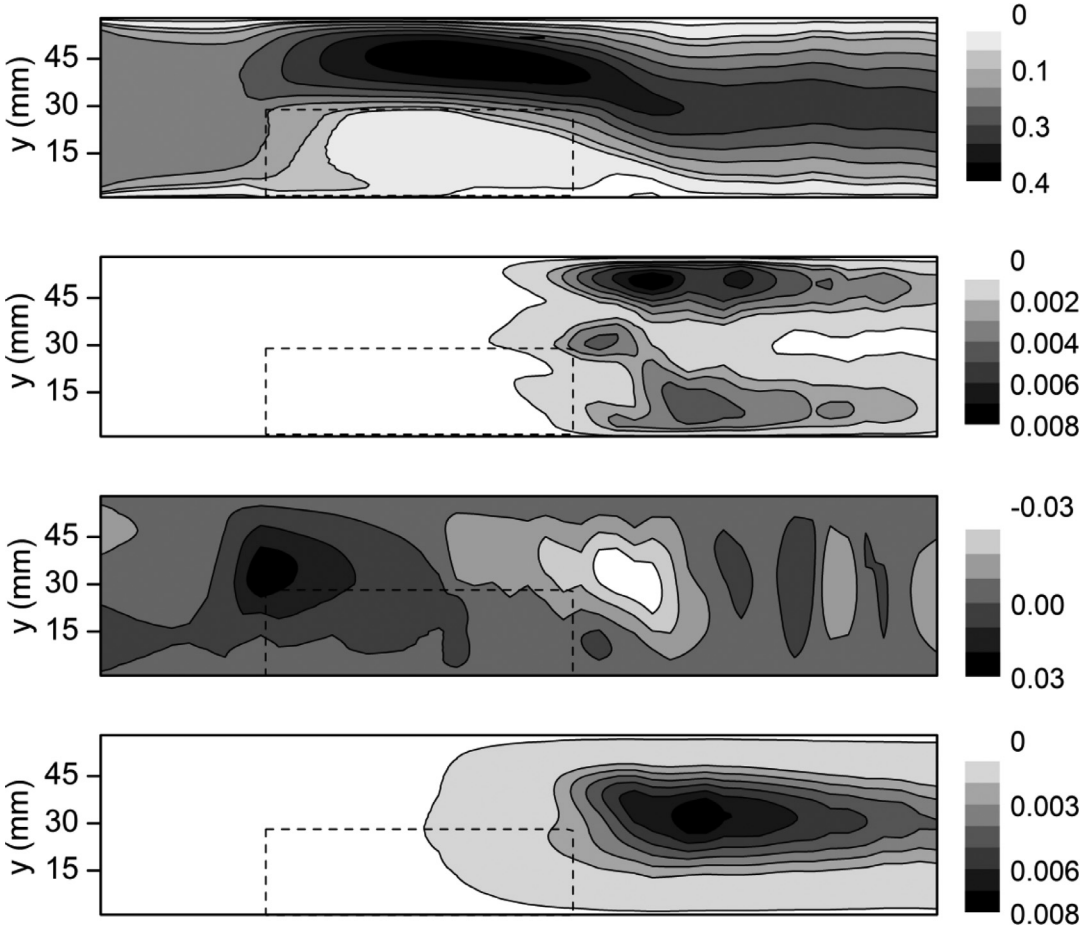

Fig. 4. Contour maps calculated for the lateral configuration. From top to bottom: mean and standard deviation of the stream-wise component of the velocity (u_x), mean and standard deviation of the transversal velocity (u_y). The dashed lines indicate the wired region.

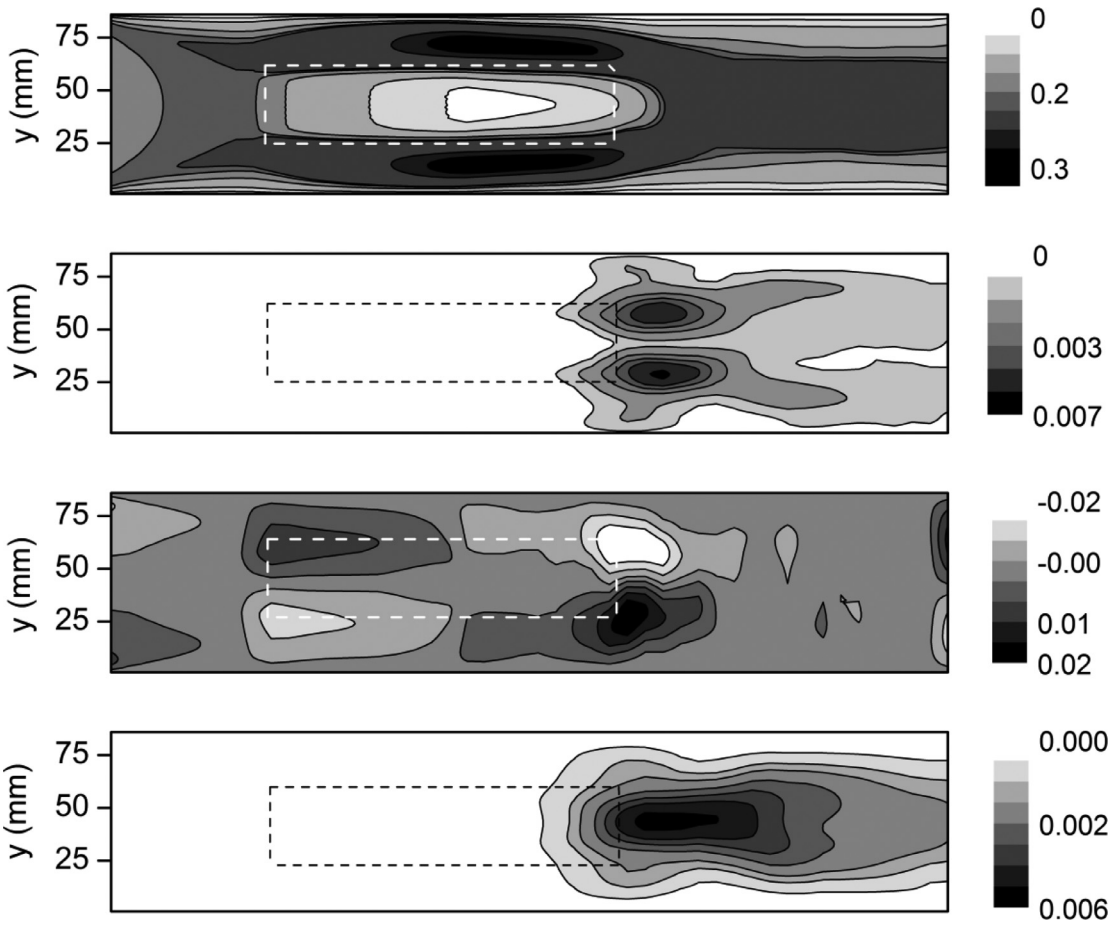

Fig. 5. Contour maps calculated for the central configuration. From top to bottom: mean and standard deviation of the stream-wise component of the velocity (u_x), mean and standard deviation of the transversal velocity (u_y). The dashed lines indicate the wired region.

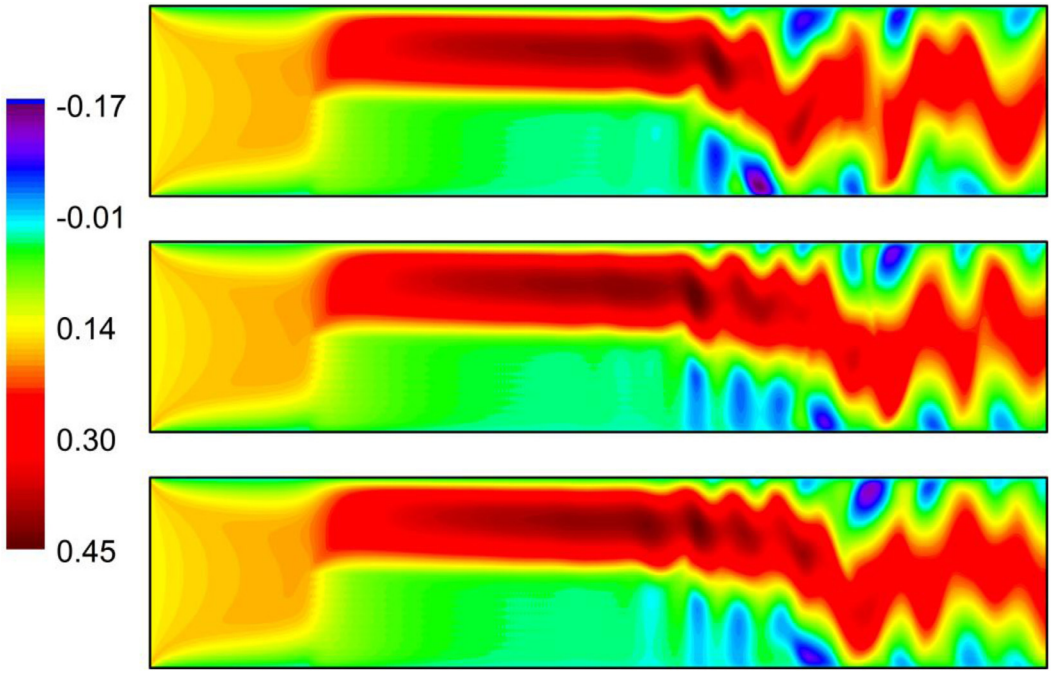

Fig. 6. Sequences of contour plots of the velocity magnitude taken at different times (lateral configuration).

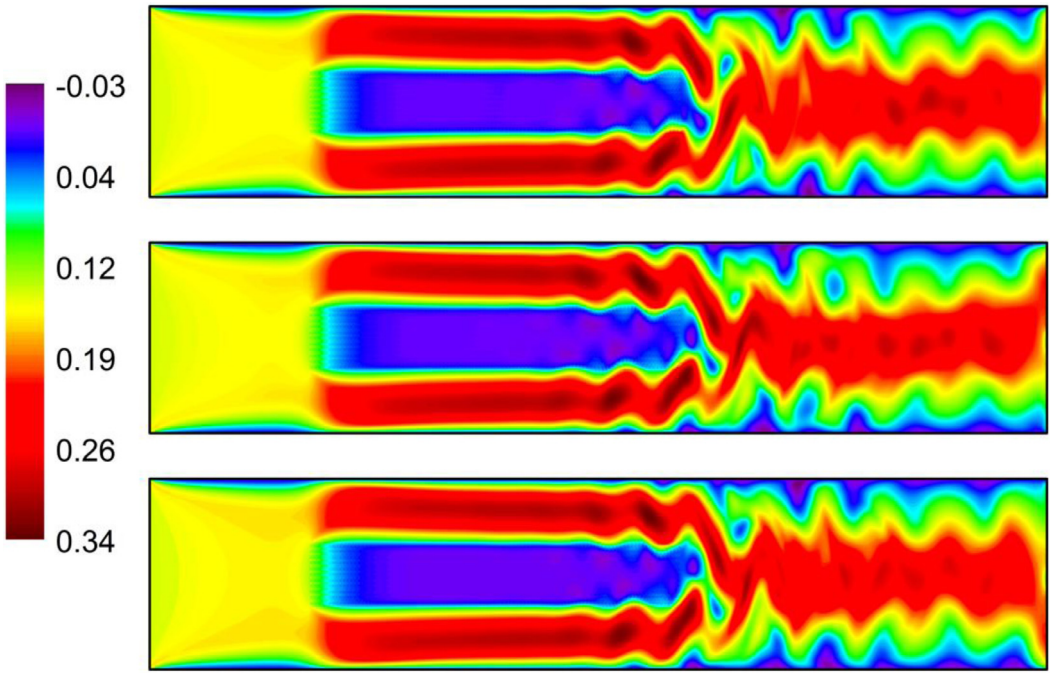

Fig. 7. Sequences of contour plots of the velocity magnitude taken at different times (central configuration).

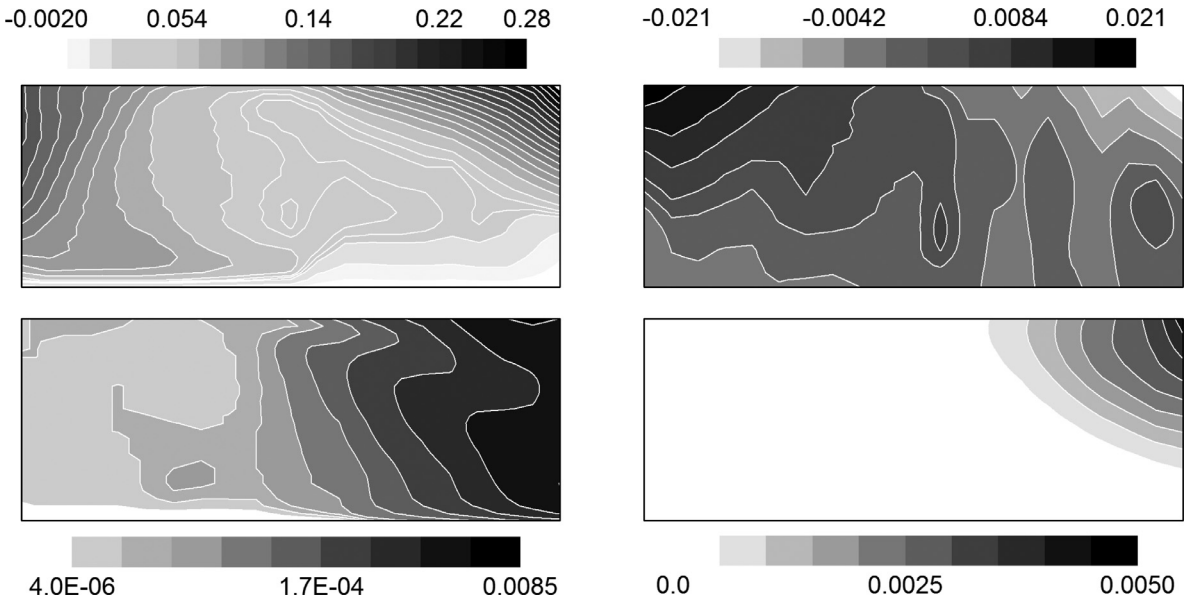

Fig. 8. Contour maps calculated inside the wired region of the lateral configuration. Left: average stream-wise component of the velocity u_x (top) and its standard deviation (bottom). Right: transversal component of the velocity, u_y (top) and its standard deviation (bottom).

for each configuration. The higher stream-wise velocities (darker areas) occur in both geometries at the free flow paths around the wired regions, whereas the lower levels (lighter areas) occur amid the wires. In the lateral case there is a region of very small negative stream-wise velocity adjacent to the lower wall in the lee of the obstacles, indicating a recirculation vortex. The latter is also confirmed by the spot of negative (downward) transversal velocity at the end of the wired region. The regions of higher perturbations after the obstruction are consistent with the flow expansion.

Figs. 6 and 7 show sequences of contour plots of the velocity magnitude taken at different times where it can be seen how the model captures the oscillatory character of the flow. The fluctuations grow in the axial direction, which is consistent with shear flow instabilities [24], and become more intense as the flow leaves the permeable obstruction, due to the sudden expansion of the free-flow section in that region. This creates a strong vortex shedding flow in the lee that produce negative velocity spots near the walls. It is interesting also to observe the effect of individual wires on the velocity at the front of the obstructions.

In many natural and technological situations, the characteristics of the flow amid permeable arrays like the ones studied here are of great interest, for the source or sink of scalars (heat, chemical species, pollen, etc.) are located in this region. Figs. 8 and 9 map in more detail the average velocity and amplitude of the fluctuations inside the wired regions. Fig. 10 shows the correspondent current lines of the average velocity field inside the wired region in each configuration. In the lateral configuration (Fig. 8) the first remarkable feature is the negative stream-wise velocity near the bottom left side of the

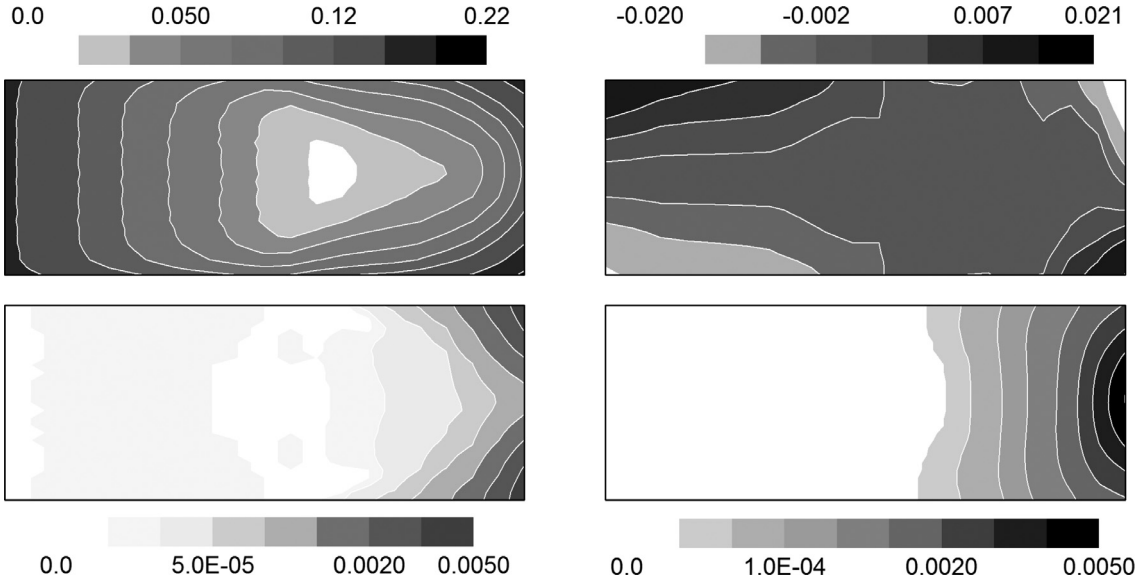

Fig. 9. Contour maps calculated inside the wired region of the central configuration. Left: average stream-wise component of the velocity u_x (top) and its standard deviation (bottom). Right: transversal component of the velocity, u_y (top) and its standard deviation (bottom).

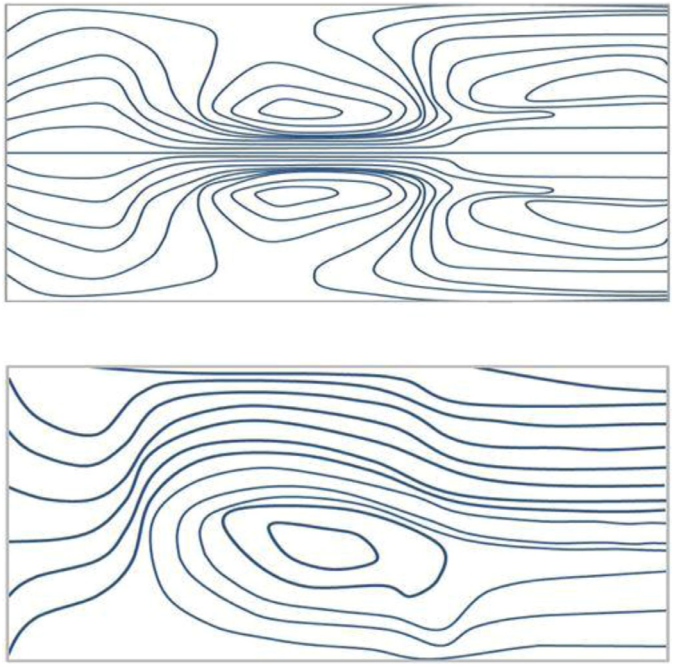

Fig. 10. Current lines of the average velocity field amid the wired region of the central (top) and lateral (bottom) configurations.

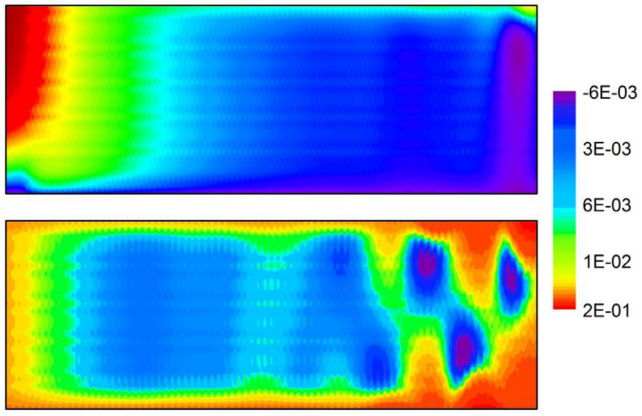

Fig. 11. Contour plots of a snapshot of the velocity magnitude inside the wired regions, lateral configuration (top), central configuration (bottom).

obstructed region, caused by a recirculation bubble that penetrates deeply inside the wired region from below. Fig. 10 shows clearly this recirculation and also a vortex that develops in the center of the region. It is also observed that the velocity fluctuations increase in magnitude in the stream-wise direction. In the central configuration (Fig. 9) there is a central stagnation spot characterized by almost null velocity and velocity fluctuations. This is not obvious for a permeable obstruction and is the result of a complex vortex structure that can be seen in Fig. 10, which causes equalization of pressure gradients. This phenomenon might be useful for locating critical items that require stagnation conditions, or explaining natural developments that might be favored by these flow conditions.

Fig. 11 shows instantaneous snapshots of the velocity magnitude amid the wired regions in both configurations. It can be seen that negative velocity spots arise in both cases, similar to the Von Karman vortex street in the back open region of the central configuration. These well-known flow features usually appear in the lee of solid obstructions. In the present permeable obstructions they occupy part of the obstructed region as well.

3.1. Cross correlations

The correlation of the velocity at different spatial locations is a good indicator to test the capabilities of the numerical model to capture the dynamic features of the flow in semi-permeable channels like the ones experimentally studied in the present work. The cross correlation provides statistical information on the phase and amplitude of the flow fluctuations as well as the flow structures that bring about the fluctuations. Accordingly, two sensors were placed in different axial positions to obtain simultaneously the two velocities. A hot-wire sensor was placed at a position x_1 100 mm upstream from the permeable block end and was moved by means of a calibrated screw in a sequence of positions, y_1, separated 2 mm from each other

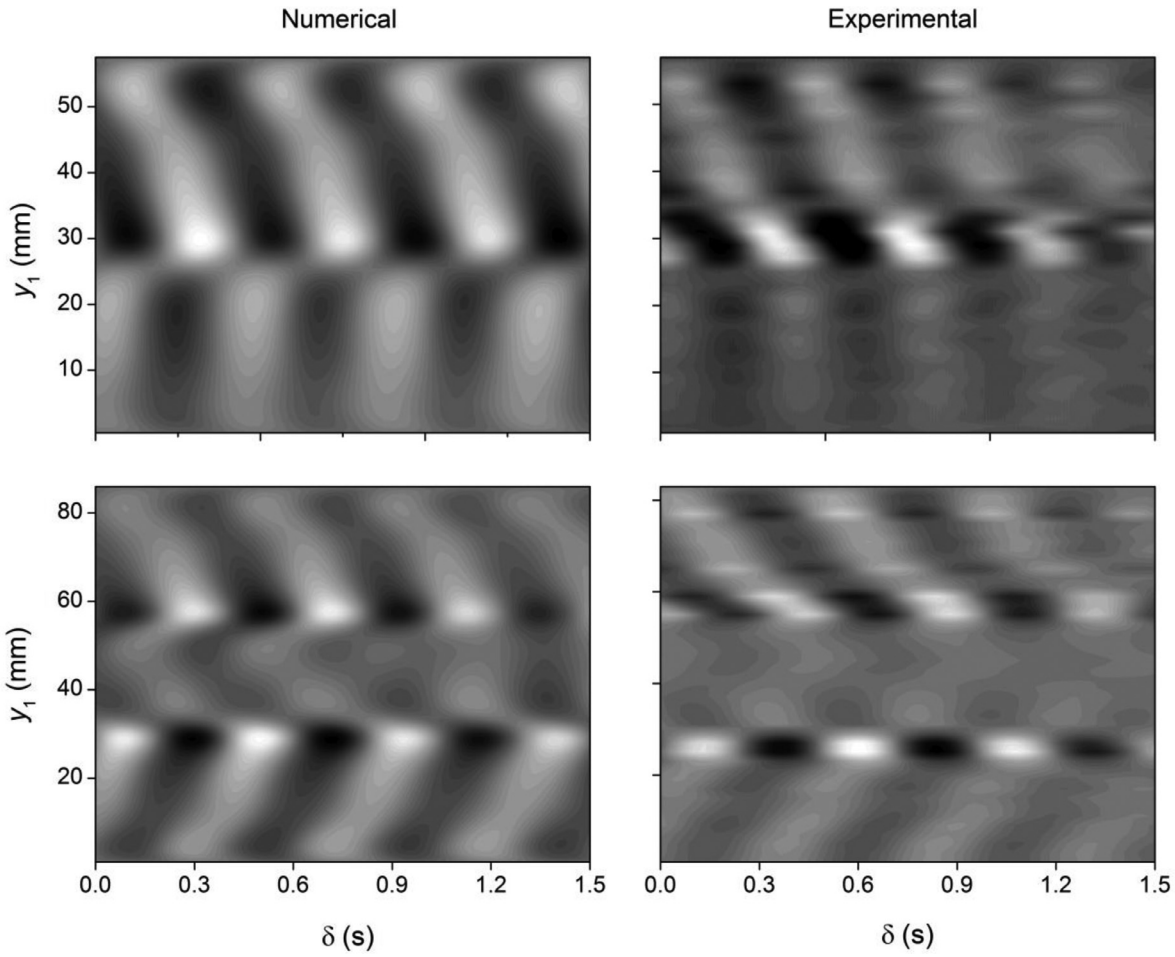

Fig. 12. Numerical and the experimental cross correlation between probes S_o and S_1 (see Fig. 1), for the lateral (top) and central configuration (bottom).

in the transversal direction. Another reference anemometer was located at a fixed axial position, x_o, 50 mm downstream from x_1, and at a fixed transversal position, y_o, in the upper free flow zone 7 mm from the permeable block border. Both signals were cross correlated and the results were normalized with the standard deviation of the signals obtained at the same transversal position, that is:

$$C(\delta, y_1) = \frac{\frac{1}{T}\int_0^T u_x(x_o, y_o, t+\delta)u_x(x_1, y_1, t)dt - \frac{1}{T^2}\left(\int_0^T u_x(x_o, y_o, t)\,dt\right)\left(\int_0^T u_x(x_1, y_1, t)dt\right)}{\sigma_o \sigma_1} \tag{16}$$

$$\sigma_o = \sqrt{\frac{1}{T}\int_0^T u_x^2(x_o, y_o, t)\,dt - \left(\frac{1}{T}\int_0^T u_x(x_o, y_o, t)\,dt\right)^2} \tag{17}$$

$$\sigma_1 = \sqrt{\frac{1}{T}\int_0^T u_x^2(x_1, y_o, t)\,dt - \left(\frac{1}{T}\int_0^T u_x(x_1, y_o, t)\,dt\right)^2}. \tag{18}$$

Fig. 12 compares the numerical and the experimental results for each configuration. It can be seen that the general trends are very similar, both showing that the correlation is lower in the wired region and in the center of the open flow layers, whereas the highest values occur in the open-flow layer close to the boundary with the permeable region. Moreover, the correlation lobes deform to smaller delay times δ from the boundary into the open flow layer. This is consistent with the downstream propagation of the fluctuations. In the lateral case, within the permeable layer, there is a phase difference between the experimental and the numerical results. A similar situation is observed in the lower half of the permeable layer in the central case. The reason for these discrepancies is not clear but seems to have only minor effects on the overall flow characteristics.

5. Conclusion

Unstable gas flows in a channel partially obstructed by an array of wires were simulated by means of a lattice Boltzmann scheme. The wired region was modeled by coupling the structure with the fluid through forces following the interpolation procedure of the immersed boundary method. The present method differs from the latter in that the structure is represented by volumetric arrays of fixed points that exert reactive forces governed by the Darcy law and not by elastic kinematics.

The model was validated against two experiments consisting of air flowing in a channel partially obstructed by arrays of wires, namely, a symmetrical and a lateral configuration. The resulting oscillatory structures were characterized by the cross correlation of the local velocity at separate points, finding good agreement between model and experiment.

In the simulations the permeability κ of the wire array was set to 1.45 10^{-4} m^2, which stems from the fitting of the measured average velocities, resulting the same value for both arrangements. It is worth noting that the overall Reynolds number varies substantially between the two cases studied. Furthermore, the velocity fluctuations obtained in the simulations with a single permeability are also in qualitative and quantitative agreement with the experimental results.

References

[1] Boroni G, Dottori J, Dalponte D, Rinaldi P, Clausse A. An improved immersed-boundary algorithm for fluid-solid interaction in Lattice-Boltzmann simulations. Latin Am Appl Res 2013;43:181–7.
[2] Chang HW, Hong PY, Lin LS, Lin CA. Simulations of flow instability in three dimensional deep cavities with multi relaxation time Lattice-Boltzmann method on graphic processing units. Comput. Fluids 2013;88:866–71.
[3] Coppola G, Gomez A. Experimental investigation on a turbulence generation system with high-blockage plates. Exp Therm Fluid Sci 2009;33:1037–48.
[4] Dalponte D, Silin N, Clausse A. Gas flow in a channel semiobstructed by a porous media. J Porous Media 2012;15:927–36.
[5] Finnigan JJ. Turbulence in Plant Canopies. Ann Rev. Fluid Mech. 2000;32:519–71.
[6] Gayev Y. Variety of problems associated with canopies. Flow and transport processes with complex obstructions I.. The Netherlands: Springer; 2004.
[7] Grucelski A, Pozorski J. Lattice-Boltzmann simulations of flow past a circular cylinder and in simple porous media. Comput Fluids 2013;71:406–16.
[8] Guo X, Zhong C, Zhuo C, Cao J. Multiple-relaxation-time lattice Boltzmann method for study of two-lid-driven cavity flow solution multiplicity. Theor Comp Fluid Dyn 2013;28:215–31.
[9] He X, Luo LS. Theory of the lattice Boltzmann method: From the Boltzmann equation to the lattice Boltzmann equation. Phys Rev E 1997;56:6811–17.
[10] Huang H, Huang JJ, Lu XY. Study of immiscible displacements in porous media using a color-gradient-based multiphase lattice Boltzmann method. Comput Fluids 2014;93:164–72.
[11] Kao TW, Park C. Experimental investigations of the stability of channel flows – Part 1. Flow of a single liquid in a rectangular channel. J Fluid Mech. 1970;43:145–64.
[12] Larson RE, Higdon JJL. Microscopic flow near the surface of two-dimensional porous media. Part I. Axial flow. J Fluid Mech 1986;166:444–72.
[13] Lopez F, Garcia MH. Mean flow and turbulence structure of open-channel flow through non-emergent vegetation. J Hydraul Eng 2001;127:392–402.
[14] Merzari E, Wang S, Ninokata H, Theofilis V. Biglobal linear stability analysis for the flow in eccentric annular channels and a related geometry. Phys Fluids 2008;20:114104.
[15] Meyer L. From discovery to recognition of periodic large scale vortices in rod bundles as source of natural mixing between sub channels – A review. Nucl Eng Des 2010;240:1575–88.
[16] Mohamad A, Kuzmin A. A critical evaluation of force term in lattice Boltzmann method, natural convection problem. Int. J. Heat Mass Transfer 2010;53:990–6.
[17] Osorio O, Silin N, Converti J. Fabrication of hot-wire probes and electronics for constant temperature anemometers. Latin Am Appl Res 2010;40:233–9.
[18] Ozalp C, Pinarbasi A, Sahin B. Experimental measurement of flow past cavities of different shapes. Experim Therm Fluid Sci 2010;34:505–15.
[19] Pan C, Luo LS, Miller CT. An evaluation of lattice Boltzmann schemes for porous medium flow simulation. Comput Fluids 2006;35:898–909.
[20] Peskin CS. The immersed boundary method. Acta Numerica 2002;11:479–517.
[21] Poggi V, Katul GG. Micro and macro dispersive fluxes in canopy flows. Acta Geophysica 2008;56:778–800.
[22] Qian YH, d'Humieres Q, Lallemand P. Lattice BGK Models for Navier–Stokes Equation. Euro phys Lett 1992;17:479–84.
[23] Raupach MR, Finnigan JJ, Brunet Y. Coherent eddies and turbulence in vegetation canopies: The mixing-layer analogy. Boundary-Layer Meteorol 1996;78:351–82.
[24] Silin N, Converti J, Dalponte D, Clausse A. Flow instabilities between two parallel planes semi-obstructed by an easily penetrable porous medium. J Fluid Mech 2011;689:417–33.
[25] Socolofsky SA, Jirka GH. Large-scale flow structures and stability in shallow flows. J Environ Eng Sci 2004;3:451–62.
[26] Sukop MC, Thorne DT. Lattice Boltzmann Modeling, an introduction for geoscientists and engineers. Berlin: Springer-Verlag; 2006.
[27] Vidal D, Roy R, Bertrand F. On improving the performance of large parallel lattice Boltzmann flow simulations in heterogeneous porous media. Comput Fluids 2010;39:324–37.
[28] White BL, Nepf HM. Shear instability and coherent structures in shallow flow adjacent to a porous layer. J Fluid Mech 2007;593:1–32.
[29] Yeomans JM. Mesoscale simulations: Lattice Boltzmann and particle algorithms. Phys A 2006;369:159–84.
[30] Zou Q, He X. On pressure and velocity boundary conditions for the lattice Boltzmann BGK model. Phys Fluids 1997;9:1591–8.